A Comparison of CMIP3 Simulations of Precipitation over North America with Observations: Daily Statistics and Circulation Features Accompanying Extreme Events

ANTHONY M. DEANGELIS, ANTHONY J. BROCCOLI, AND STEVEN G. DECKER

Department of Environmental Sciences, Rutgers, The State University of New Jersey, New Brunswick, New Jersey

(Manuscript received 21 June 2012, in final form 12 October 2012)

ABSTRACT

Climate model simulations of daily precipitation statistics from the third phase of the Coupled Model Intercomparison Project (CMIP3) were evaluated against precipitation observations from North America over the period 1979–99. The evaluation revealed that the models underestimate the intensity of heavy and extreme precipitation along the Pacific coast, southeastern United States, and southern Mexico, and these biases are robust among the models. The models also overestimate the intensity of light precipitation events over much of North America, resulting in fairly realistic mean precipitation in many places. In contrast, heavy precipitation is simulated realistically over northern and eastern Canada, as is the seasonal cycle of heavy precipitation over a majority of North America. An evaluation of the simulated atmospheric dynamics and thermodynamics associated with extreme precipitation events was also conducted using the North American Regional Reanalysis (NARR). The models were found to capture the large-scale physical mechanisms that generate extreme precipitation realistically, although they tend to overestimate the strength of the associated atmospheric circulation features. This suggests that climate model deficiencies such as insufficient spatial resolution, inadequate representation of convective precipitation, and overly smoothed topography may be more important for biases in simulated heavy precipitation than errors in the large-scale circulation during extreme events.

1. Introduction

Climate models are useful tools for quantifying and understanding changes in climate that may occur in response to natural and anthropogenic warming. Extreme precipitation events, due to their ability to cause widespread property damage and loss of life (Easterling et al. 2000; Rappaport 2000; USGS 2006), are among the more important phenomena that climate models are used to study. Using climate models to predict and understand changes in extreme precipitation events requires that the models realistically simulate the statistics of high-frequency precipitation as well as the physical mechanisms that generate heavy precipitation. It is therefore important that the precipitation output from climate models be evaluated against high-quality observations over the twentieth century.

Several previous studies have evaluated climate model simulations of daily and higher-frequency precipitation. Despite differences among the studies regarding the models and observations used, geographical domain analyzed, and quantitative methods, many of the same model biases were found over various regions: too many wet days, overestimation of the frequency and intensity of light precipitation events, and underestimation of the frequency and intensity of heavy events (e.g., Zwiers and Kharin 1998; Iorio et al. 2004; May 2004; Emori et al. 2005; Kimoto et al. 2005; Kharin et al. 2007; Perkins et al. 2007; Sun et al. 2007; Wehner et al. 2010). Such biases in simulated precipitation were found not only with coarse-resolution climate models but also high-resolution regional models (Frei et al. 2003; Gutowski et al. 2003; Semmler and Jacob 2004; Boroneant et al. 2006; Lenderink and van Meijgaard 2008; Boberg et al. 2009). In one study, high-resolution regional models were shown to overestimate heavy and extreme precipitation over much of the contiguous United States (Wehner 2013). In the studies referenced above, model biases existed whether observations were treated as station point values or gridded at a resolution comparable to the climate models studied.

Several studies have shown that when climate models are run at higher spatial resolution, the simulation of

Corresponding author address: Anthony DeAngelis, Department of Environmental Sciences, Rutgers University, 14 College Farm Road, New Brunswick, NJ 08901.
E-mail: deangelis@envsci.rutgers.edu

DOI: 10.1175/JCLI-D-12-00374.1

high-frequency heavy precipitation statistics improves (Iorio et al. 2004; Kimoto et al. 2005; Kharin et al. 2007; Wehner et al. 2010; Dulière et al. 2011). One reason higher-resolution climate models simulate heavy precipitation better may be that the models rely less on convective parameterizations when run at higher resolutions (Iorio et al. 2004; Wehner et al. 2010; Li et al. 2011). Previous studies imply that convective parameterizations in climate models partly result in the underestimation of intense precipitation and too frequent simulation of light events (Gutowski et al. 2003; Iorio et al. 2004; May 2004; Emori et al. 2005; Kharin et al. 2007; Wilcox and Donner 2007; Wehner et al. 2010; Li et al. 2012). Some studies have demonstrated that convective precipitation can be made more realistic by changing the characteristics of convective parameterization schemes or by embedding cloud-resolving models into climate models (Iorio et al. 2004; Emori et al. 2005; Wilcox and Donner 2007; Li et al. 2012). Other reasons for improved simulation of intense precipitation with increased horizontal resolution may include improved dynamics and vertical motion, better simulation of tropical cyclones, more realistic representation of topography, and better ability to resolve mesoscale processes and land surface–atmosphere interactions (Colle and Mass 2000; Gutowski et al. 2003; Iorio et al. 2004; Semmler and Jacob 2004; Wehner et al. 2010; Dulière et al. 2011; Li et al. 2011).

Since climate models are used to predict future changes in extreme precipitation in response to global warming, it is important to know how well climate models simulate observed changes in heavy precipitation that are associated with warming over the late twentieth century. Unfortunately, previous studies have shown that climate model simulations of observed trends in heavy precipitation are rather poor. For example, Kiktev et al. (2003) showed that HadAM3, the atmospheric component of the third climate configuration of the Met Office Unified Model (HadCM3), has little skill in reproducing observed trends in precipitation indices over the late twentieth century, such as the annual maximum five-day precipitation event. Other studies have shown that climate models underestimate observed positive trends in heavy precipitation over a variety of domains, such as Northern Hemisphere land areas (Min et al. 2011), South America (Marengo et al. 2010), Germany (Tomassini and Jacob 2009), and Australia (Alexander and Arblaster 2009). Studies have also shown that observed amplifications in tropical extreme precipitation with increased sea surface temperatures are underestimated by atmosphere-only and coupled simulations from the third phase of the Coupled Model Intercomparison Project (CMIP3) (Allan and Soden 2008; Gastineau and Soden 2011). Finally, Lenderink and van Meijgaard (2008) showed that a high-resolution regional climate model underestimates the increase in intense hourly precipitation observed with higher daily temperatures over Europe during the twentieth century. These previous studies suggest that future increases in the frequency and intensity of heavy and extreme precipitation events in response to global warming may be larger than current climate model simulations indicate.

Changes in the physical mechanisms that generate extreme precipitation, such as features of the large-scale circulation, are likely to play a role in quantitative changes in extreme precipitation in the future (Zwiers and Kharin 1998; Yin 2005; Meehl et al. 2005; Emori and Brown 2005; Lionello and Giorgi 2007; Archambault et al. 2008; Gutowski et al. 2008a,b; Gastineau and Soden 2011). Furthermore, it is possible that unrealistic climate model simulations of the large-scale atmospheric dynamics and thermodynamics associated with extreme precipitation events lead to biases in the amount of precipitation simulated. For these reasons, it is of great importance to evaluate the ability of climate models to reproduce the large-scale physical mechanisms that are observed with extreme precipitation events. While it has been shown that climate models simulate fairly realistic atmospheric circulation patterns associated with extreme precipitation events over the Maritime Alps (Boroneant et al. 2006) and central United States (Gutowski et al. 2008b), few studies have evaluated the large-scale physical processes linked to extreme precipitation in climate models. Additional research on evaluating such physical mechanisms in a comprehensive way is therefore warranted and the present study aims to address this topic.

In this paper, an ensemble of coupled ocean–atmosphere climate models from CMIP3 is used in the evaluation of late-twentieth-century simulations of daily precipitation statistics and the physical mechanisms that generate extreme precipitation over North America. The use of 17 climate models, emphasis on the spatial patterns of precipitation statistics, and analysis of the atmospheric dynamic and thermodynamic structure associated with extreme daily precipitation provides a more comprehensive evaluation of CMIP3 simulated precipitation over North America than is currently available. In the subsequent section, the observations and climate models used for this paper as well as general methods are described. The main results for precipitation statistics are presented and discussed in section 3, while results for physical mechanisms are given in section 4. A summary and conclusions are provided in section 5.

2. Data and methodology

a. Precipitation observations

Gridded observations of daily precipitation covering all global land areas and the time period 1979 to present have been developed by the Climate Prediction Center (CPC). The gridded precipitation product is produced from rain gauge observations over global land areas. The stations used in the gridded product include a combination of special collections from the CPC as well as stations from the Global Telecommunications System (GTS) (Chen et al. 2008a). A quality control procedure utilizing satellite data and numerical model output was applied to the station data before gridding (Chen et al. 2008b), which was an improvement to the quality control used for the CPC U.S. precipitation product described in Higgins et al. (2000). After applying the quality control procedure, the station data were placed on a 0.5° × 0.5° longitude–latitude grid using optimal interpolation. A comparison of optimal interpolation with other gridding methods for this precipitation product is provided in Chen et al. (2008c) and reveals no significant differences between methods. We further converted the 0.5° × 0.5° grid of the observations to a 2.5° × 2.5° grid via area averaging to be more comparable with the typical resolution of the climate models analyzed (see section 2c) before computing precipitation statistics, a procedure that has been shown to improve agreement between observed and simulated metrics involving extreme precipitation (Chen and Knutson 2008). Precipitation analyses shown in this paper focus on North America because of the high density and large number of stations that went into the CPC gridded product over this region during the late twentieth century (Chen et al. 2008a,c). Precipitation data are missing for some days over parts of North America; however, because the percentage of missing days at any grid cell is no more than 0.5% over the analysis period (1979–99), the missing data should not impact the results of this paper.

b. North American Regional Reanalysis

The National Centers for Environmental Prediction (NCEP) North American Regional Reanalysis (NARR; Mesinger et al. 2006) was used as observed data for variables other than precipitation for the evaluation of large-scale atmospheric patterns associated with extreme precipitation. We regridded the NARR from its initial spatial resolution of 32 km × 32 km on a Lambert conformal conic projection to a 2.5° × 2.5° resolution to match the grid on which the precipitation observations and climate models were analyzed. A linear average of all values whose grid cell centers on the original NARR grid fell within the boundaries of the new 2.5° × 2.5° grid determined the values on the coarser grid. Furthermore, three-hourly NARR data were converted to daily averages over the daily period 1200 to 1200 UTC to match the CPC precipitation observations.

c. Climate model output

The climate model simulations evaluated in this paper were twentieth-century runs from the CMIP3 collection. These simulations were forced with realistic temporal variations of anthropogenic and natural forcings as deemed appropriate by the individual modeling groups (Meehl et al. 2007). The output from the CMIP3 models is available at the World Climate Research Programme's (WCRP's) CMIP3 multimodel dataset archive hosted by the Program for Climate Model Diagnosis and Intercomparison (http://www-pcmdi.llnl.gov/ipcc/about_ipcc.php). There were 17 models with sufficient daily precipitation output for the evaluation of precipitation statistics in this paper, and those models are listed in Table 1 (note that expansions of all CMIP3 model acronyms are available online at http://www-pcmdi.llnl.gov/ipcc/model_documentation/ipcc_model_documentation.php). Of those 17 models, only 12 had archived meteorological variables other than precipitation for use in evaluating physical mechanisms associated with heavy precipitation events; such models are also identified in Table 1. Because of the limited availability of multiple ensemble members, only one twentieth-century ensemble member run was analyzed from each model (see Table 1).

The output from each climate model was regridded to the 2.5° × 2.5° grid on which the precipitation observations and NARR output were analyzed. The regridding procedure consisted of either linear interpolation if the original climate model grid area (in square degrees) was larger than that of the target grid or area averaging otherwise. The specific models that were regridded using area averaging are shown in Table 1, along with the original horizontal resolution of all models. Because the original spatial resolution of some models is much coarser than 2.5° × 2.5°, the sensitivity of the results to the resolution of the analysis grid was evaluated by performing a parallel analysis of precipitation statistics using a 5.0° × 5.0° analysis grid. While in some cases there was better agreement between the models and observations on the 5.0° × 5.0° grid, the improvement was rather small and most of the same model biases remained. All analyses shown in this paper are therefore presented on the 2.5° × 2.5° common grid.

d. General analysis methods

The time period with the greatest overlap among the CPC observations, NARR, and CMIP3 models is 1 January 1979–31 December 1999. Because of inconsistencies in

TABLE 1. List of the CMIP3 models used for analysis in this paper. All 17 models were used for the analysis of precipitation statistics. Because of output availability, only the 12 models with asterisks next to the model name were included in the analysis of physical mechanisms associated with extreme precipitation events. The approximate spatial resolutions were calculated by dividing 360° or 180° by the number of grid cells in the longitude or latitude dimensions, respectively. Asterisks next to spatial resolution denote climate models whose grids were transformed to the common 2.5° × 2.5° resolution using area averaging. All others were transformed using linear interpolation. The ensemble member number used for each model is indicated. [Further documentation for individual models, including expansions of all acronyms, is available online at http://www-pcmdi.llnl.gov/ipcc/model_documentation/ipcc_model_documentation.php.]

Modeling group	Country	Model name	Run	Spatial resolution (lon × lat)
Canadian Centre for Climate Modeling and Analysis	Canada	CCCMA-CGCM3.1(T47)*	1	3.75° × 3.75°
		CCCMA-CGCM3.1(T63)*	1	2.81° × 2.81°
Centre National de Recherches Météorologiques	France	CNRM-CM 3*	1	2.81° × 2.81°
CSIRO Atmospheric Research	Australia	CSIRO-Mk3.0*	1	1.88° × 1.88°*
		CSIRO-Mk-3.5*	1	1.88° × 1.88°*
Geophysical Fluid Dynamics Laboratory	USA	GFDL-CM2.0*	1	2.50° × 2.00°*
		GFDL-CM2.1*	2	2.50° × 2.00°*
Goddard Institute for Space Studies	USA	GISS-AOM*	1	4.00° × 3.00°
		GISS-EH*	5	5.00° × 3.91°
		GISS-ER*	1	5.00° × 3.91°
Institute of Atmospheric Physics	China	IAP-FGOALS-g1.0	1	2.81° × 3.00°
Institute for Numerical Mathematics	Russia	INM-CM3.0	1	5.00° × 4.00°
Center for Climate System Research, National Institute for Environmental Studies, and Frontier Research Center for Global Change	Japan	MIROC3.2(medres)	1	2.81° × 2.81°
Max Planck Institute for Meteorology	Germany	MPI-ECHAM5*	1	1.88° × 1.88°*
Meteorological Research Institute	Japan	MRI-CGCM2.3.2*	1	2.81° × 2.81°
National Center for Atmospheric Research	USA	NCAR-CCSM3	1	1.41° × 1.41°*
		NCAR-PCM	1	2.81° × 2.81°

the calendar setup among the CMIP3 models, 29 February was removed from all datasets, resulting in a time domain of exactly 7665 days for the CPC and NARR observations and all CMIP3 models. The 1979–99 time period of analysis was considered too short for long-term trends in precipitation statistics to be reliable, so only summary statistics over this period were analyzed. This decision was based on an analysis we performed using the CPC U.S. precipitation dataset (Higgins et al. 2000) over the period 1961–98, which showed that long-term trends in daily precipitation statistics are spatially noisy and unlikely to be statistically significant or meaningful over time periods as short as the one used in this paper (not shown).

While many studies involving extreme precipitation utilize metrics based on generalized extreme value (GEV) or other statistical distributions (e.g., Zwiers and Kharin 1998; Wilby and Wigley 2002; May 2004; Semmler and Jacob 2004; Kharin and Zwiers 2005; Kharin et al. 2007; Wehner et al. 2010; Wehner 2013), rather simple statistical methods were used in this paper. The choice of simple statistical methods was made to eliminate the potential uncertainties resulting when making the necessary assumptions involved in more sophisticated statistical procedures (Kharin and Zwiers 2005; Wehner et al. 2010; Wehner 2013). Finally, the intent of this paper is to evaluate the collective performance of the CMIP3 models and to see the range of model variability where appropriate, rather than to evaluate the individual performance of certain models. Therefore, the figures focus on the model average and the envelope of variability among the models and the results from individual models are not displayed. A detailed analysis of why certain models perform better than others requires a controlled experiment in which only certain model components are allowed to vary, which was not possible in the present study. Furthermore, it is very difficult to identify one single climate model that outperforms all others at everything (Perkins et al. 2007); therefore, a ranking of the CMIP3 models may not provide much insight.

3. Precipitation statistics

The first metric that was evaluated in the CMIP3 models was the mean daily precipitation for the analysis period 1979–99 (Fig. 1). This analysis reveals that although the models generally capture the spatial patterns of mean precipitation fairly well, they tend to underestimate precipitation in wet areas and overestimate precipitation in dry areas. For example, the model average is drier than observations by as much as 5 mm day^{-1}

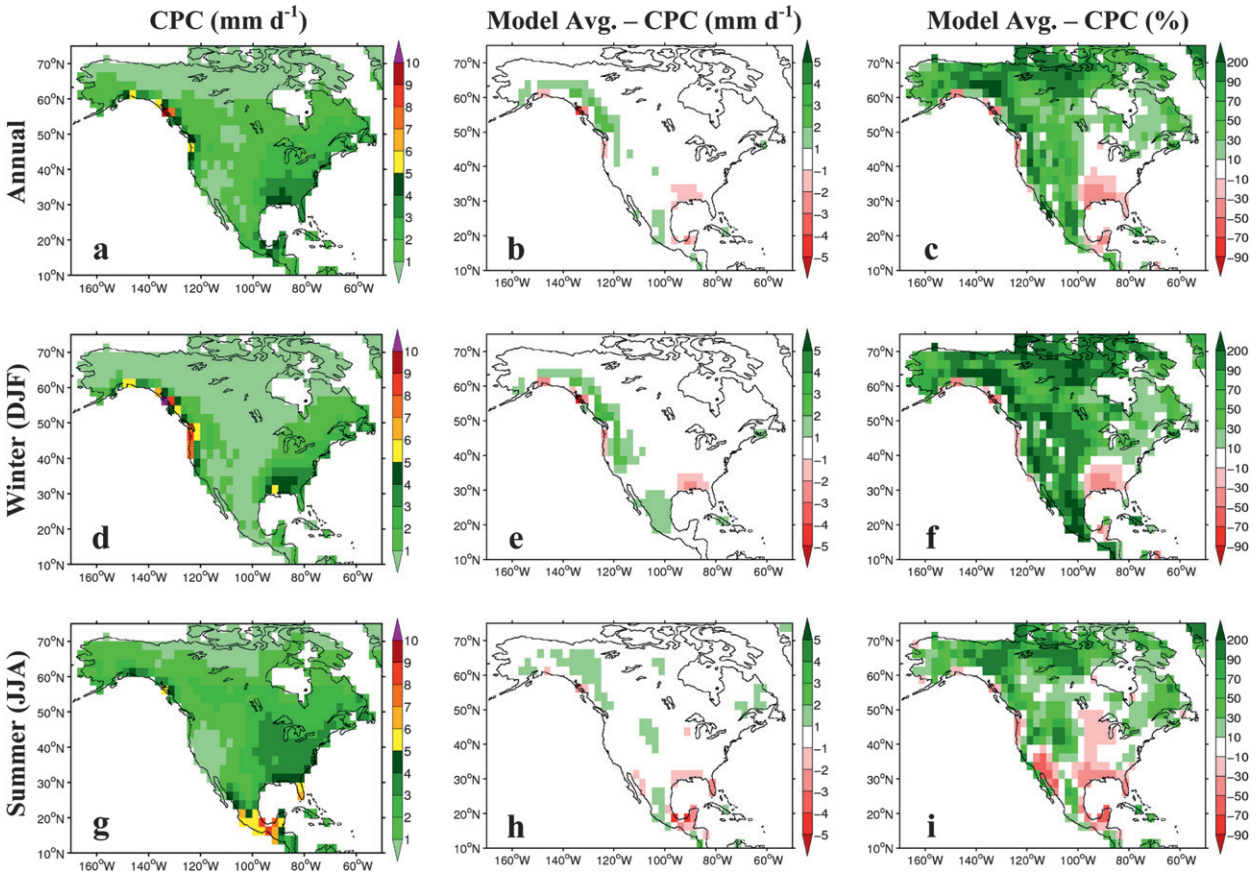

FIG. 1. Daily mean precipitation over the period 1979–99 at each grid cell on the 2.5° grid for (a)–(c) all seasons, (d)–(f) winter, and (g)–(i) summer. (left) Mean precipitation for the CPC observations, (middle) the difference between the CMIP3 model average and CPC in units of mm day^{-1}, and (right) the percent difference between the CMIP3 model average and CPC.

along the Pacific coast near 55°N during winter, where the climatological precipitation exceeds 10 mm day^{-1} (Figs. 1d,e). To the east of this area and extending a greater distance along the coast, the climatological winter precipitation is substantially lighter and the model average has wet biases of about 1–4 mm day^{-1} (Fig. 1e). Another example of substantial model dry biases over a relatively moist region is in southern Mexico and along the United States Gulf Coast, where the models are drier than observations by about 1–5 mm day^{-1} depending on location and season (Figs. 1b,e,h). The model biases in mean precipitation are consistent with those found in Iorio et al. (2004) over the contiguous United States using the National Center for Atmospheric Research (NCAR) Community Climate Model version 3 (CCM3) atmospheric general circulation model. Differences between the model average and observations are expressed as a percentage on the right column of Fig. 1 to assess how model biases scale with mean precipitation and for a more sensitive determination of the sign of model biases where the biases are small in magnitude. It appears that the model dry biases in the south and along parts of the Pacific Coast are somewhat proportional to the CPC mean precipitation, as the percent biases mostly fall between −30% and −70% in these areas (Figs. 1c,f,i). Note that much of the large area of model wet biases across the northern and interior parts of the domain when expressed as a percentage is greatly exaggerated by the calculation method and very light climatological precipitation over this area. Over much of the northeastern part of the domain, where amount and percentage biases are both small, the models simulate mean precipitation quite well.

A similar analysis was performed for the mean precipitation that falls from just the wettest 1% of days (i.e., the mean precipitation coming from the daily 99th percentile and above). This quantity (hereafter referred to as P99M) was chosen instead of the 99th percentile itself because it is likely to be less spatially noisy and represents the average intensity of heavy to extreme precipitation. The results of this analysis are displayed in Fig. 2. The average performance of the CMIP3 models is

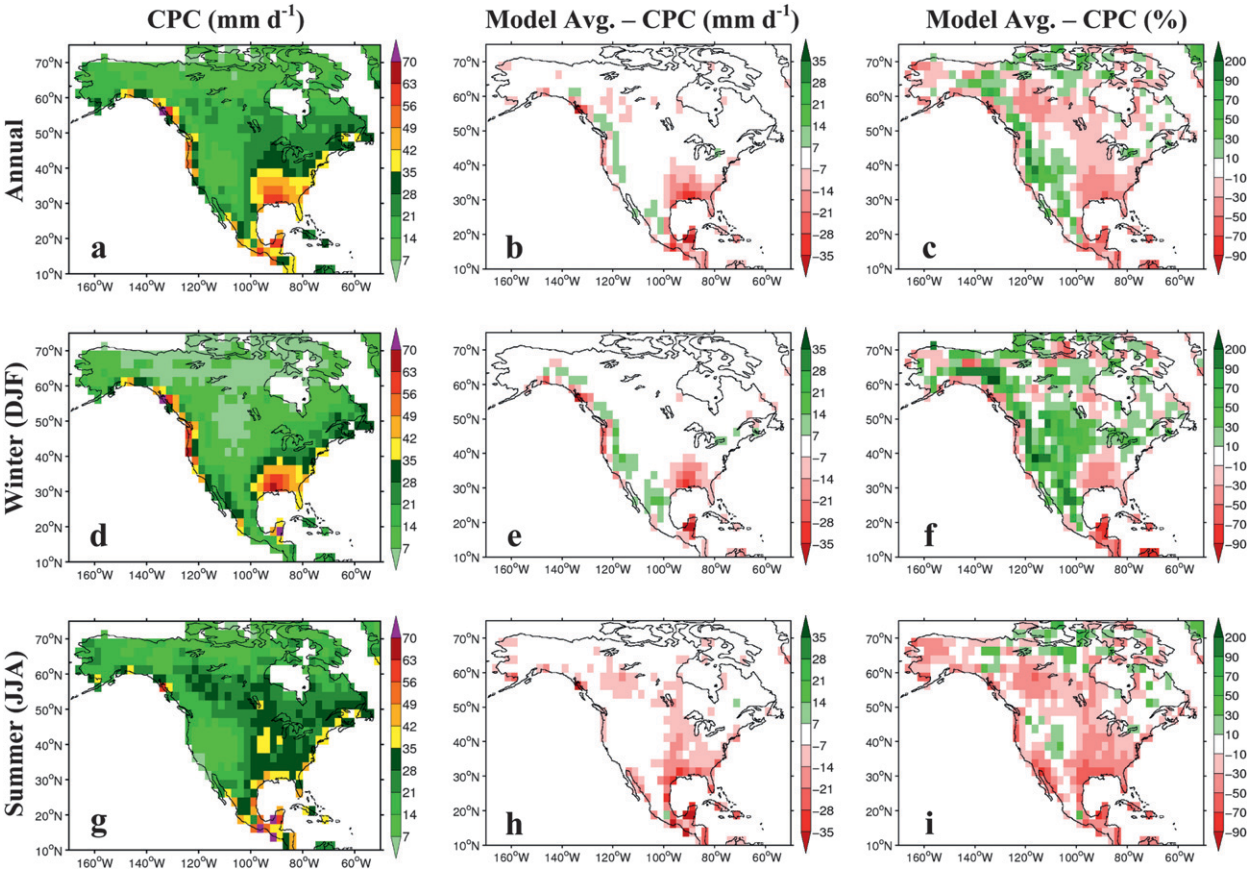

FIG. 2. As in Fig. 1, but for the mean precipitation falling from the wettest 1% of days (P99M, as defined in the text).

noticeably poorer for P99M than it is for the mean precipitation. One particular area where model biases in P99M are disproportionately larger than those in mean precipitation is the southeastern United States and southern Mexico, where P99M is underestimated by more than 15 mm day^{-1} over much of the area (Figs. 2b,e,h). When expressed as a percentage, model dry biases over this area are larger for P99M than for mean precipitation, especially during summer and in southern Mexico (Figs. 1c,f,i, and 2c,f,i). The model dry biases in P99M in the southeast United States also extend to higher latitudes during the summer season (Figs. 2e,f,h,i), more so than they do with mean precipitation (Figs. 1e,f,h,i). In general, model biases in P99M appear to be more negative over much of the domain when compared to mean precipitation biases. As was the case with mean precipitation, the model average appears to do well generally east of 100°W and north of 40°N. Overall, the results shown in Fig. 2 are consistent with previous studies that used individual climate models and studied the contiguous United States (Iorio et al. 2004; Wehner et al. 2010).

To examine the intermodel variability of the biases in P99M, six regions within the North America study domain were chosen that approximately exhibit homogeneous characteristics of climatological precipitation as well as homogeneous CMIP3 model biases in mean and P99M precipitation (Fig. 3; note that all region names are explained in the caption). The P99M model biases were then averaged over each of these regions for each model and displayed on a box-and-whisker plot for all seasons (Fig. 4). The negative biases in P99M in the PCOAST and SEAST regions appear quite robust among the models, as more than 75% of the models show negative biases during all seasons over these regions (Figs. 4a,d). Indeed, all models analyzed show negative biases during fall in the PCOAST region and during both summer and fall in the SEAST region, suggesting that there is a systematic problem that results in too little heavy precipitation in these regions and seasons, a topic that will be discussed in section 4. Substantial and robust negative biases of about the same magnitude as those over the PCOAST region are also present over the SMEX region in winter and spring (Fig. 4f). The largest variability among the individual CMIP3 models occurs over SMEX in summer and fall, where a majority of the models have negative biases but the individual

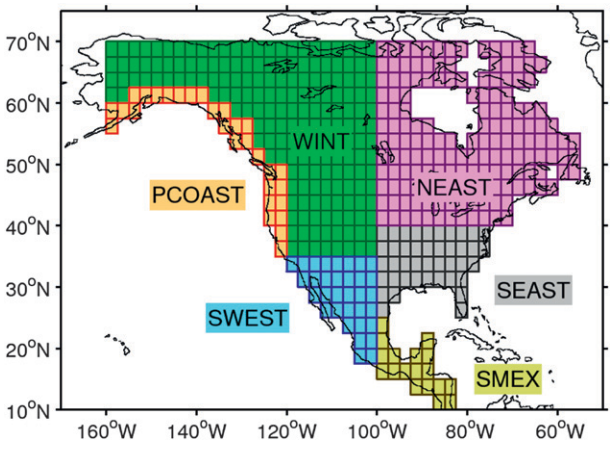

FIG. 3. Analysis regions used to study the model variability of P99M biases and daily precipitation distributions (Figs. 4 and 5, respectively). The specific 2.5° × 2.5° grid cells constituting each region are shown. The regions are named according to geographic location: Pacific coast (PCOAST), West interior (WINT), Northeast (NEAST), Southeast (SEAST), Southwest (SWEST), and southern Mexico/Central America (SMEX). Note that grid cells along the far northern, western, and eastern parts of the domain were omitted from the regions because of potential uncertainties in the CPC observations over these locations (Chen et al. 2008c).

model biases range from -40 mm day^{-1} to more than 10 mm day^{-1} (Fig. 4f). There are also robust negative model biases in the SWEST region during summer, at a time when the North American monsoon brings heavy and convective rain over parts of this region (Fig. 4e). All CMIP3 models show a positive bias over the WINT region in winter (Fig. 4b), although this bias is small in magnitude because of the light P99M precipitation over this region (Fig. 2d). The good performance of the CMIP3 models over the NEAST region is quite apparent during winter, where model biases straddle zero and have a small range of variability (Fig. 4c).

The regions defined in Fig. 3 were also used to analyze model biases over the entire daily precipitation distribution during the period 1979–99. For each grid point, daily precipitation percentiles in increments of 0.1 were computed from all days. The values of each percentile were averaged across the grid points in each of the six regions. This procedure was employed on the CPC data and the output from each of the CMIP3 models. The regional average values for each percentile from the CPC data were then paired with those from each of the CMIP3 models to form a set of quantile–quantile (Q–Q) plots, a graphical approach for comparing distributions from two samples (Wilks 2006, 113–114). The Q–Q plots shown in Fig. 5 are constructed by comparing the minimum, median, and maximum CMIP3 model value for each percentile to the corresponding CPC value to depict the envelope of model performance for that region.

Despite the details of the precipitation distributions being somewhat different over each region, Fig. 5 shows that there are aspects of the model biases that are robust for all regions. The models tend to overestimate the intensity of light precipitation events, as seen by the model median rising above the 1:1 line at the low end of the precipitation distribution in every region. At the high end of the distribution, the opposite problem occurs, whereby the models tend to underestimate the intensity of daily events to a degree that varies depending on the region. The intensity at which the model median transitions from overestimating to underestimating daily precipitation varies from as light as 2–3 mm day^{-1} over the SEAST region (Fig. 5d) to as heavy as 20 or more mm day^{-1} for regions such as NEAST and SWEST (Figs. 5c,e), depending on the severity of model biases in P99M precipitation (Figs. 2 and 4). Numerous studies have found that climate models of varying spatial resolution and complexity have similar qualitative biases in daily precipitation distributions over Northern Hemisphere land regions (Sun et al. 2007), the United States (Gutowski et al. 2003; Iorio et al. 2004), Europe (Boberg et al. 2009), Australia (Perkins et al. 2007), and Japan (Kimoto et al. 2005). The result of climate models overestimating light precipitation and underestimating heavy precipitation is that they simulate relatively realistic mean precipitation, as shown in Fig. 1 and in earlier studies (e.g., Frei et al. 2003; Iorio et al. 2004; May 2004; Kimoto et al. 2005; Boroneant et al. 2006; Dulière et al. 2011). Potential reasons for the underestimation of heavy precipitation found in climate models are discussed in section 4.

To investigate the ability of the CMIP3 models to accurately simulate the seasonality of heavy precipitation events, the seasonal cycle of heavy precipitation was objectively quantified in CPC observations and CMIP3 models using harmonic analysis. More specifically, the P99M precipitation was computed separately for each calendar month over the period 1979–99 at each grid cell, resulting in a time series with 12 elements. Then, a one-period sinusoidal function (also known as the first harmonic) was fit to this 12 element time series using least squares regression as described in Wilks (2006, 371–381). The resulting harmonic fit can be described with a phase representing the time of year of maximum P99M and the percentage of total variance of monthly P99M that is explained by the harmonic fit, which is proportional to the relative strength of the seasonal cycle of P99M. The phase is shown with vectors and percent variance with color fills in Fig. 6.

Figure 6 shows that on average, the CMIP3 models reasonably reproduce the observed seasonal patterns of heavy to extreme precipitation over most of North America, especially when considering the additional

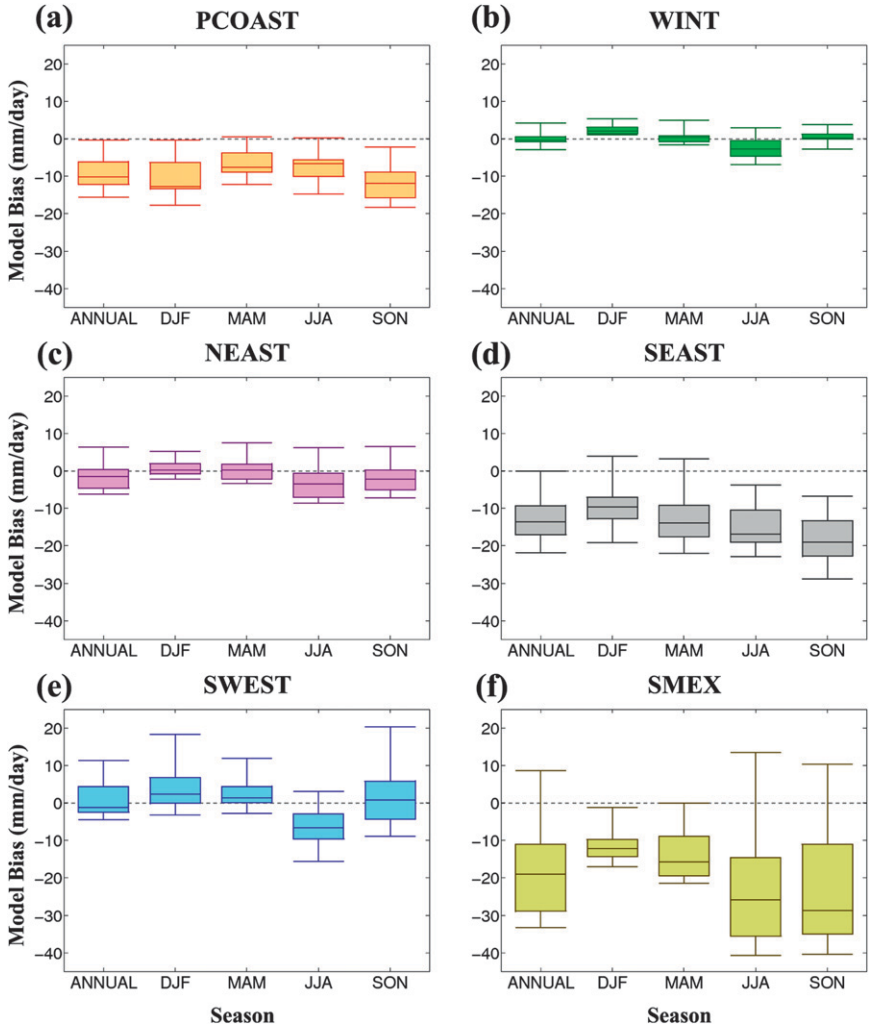

FIG. 4. Box-and-whisker plots showing the variability of CMIP3 model biases in P99M averaged over the specified regions (Fig. 3). The horizontal lines on the box and whiskers indicate the minimum, 25th percentile, median, 75th percentile, and maximum biases of the individual models.

smoothing inherent in computing a multimodel average. In particular, the strong fall-to-winter maximum along the Pacific coast, summer maximum in the northern interior, and mid-to-late summer maximum in southern Mexico are simulated reasonably accurately by the models. The apparent disagreement between the CMIP3 model average and CPC observations in parts of northern Canada may be influenced by the sparseness of observations over this area (Chen et al. 2008c). More substantial disagreements between the CMIP3 simulated and observed seasonal cycle of P99M exist over the west coast of Mexico and the southeastern United States, where the models show a stronger and more widespread cool season maximum than is observed. Such biases may be the result of the models underpredicting P99M precipitation more severely during summer than winter in these regions (Figs. 2 and 4). The models also simulate a pronounced winter maximum in P99M farther inland along the Pacific coast than is observed, which appears to be related to the overestimation of heavy winter precipitation in this region as a result of the coarse terrain representation in the models (Fig. 2). Ruiz-Barradas and Nigam (2006) used a harmonic analysis similar to the one presented here to evaluate the performance of a subset of CMIP3 models in simulating the seasonal cycle of mean precipitation over North America. While certain models in their analysis showed difficulty in simulating the correct timing and amplitude of the observed seasonal cycle over various places, the models collectively captured the presence of a notable winter maximum along the

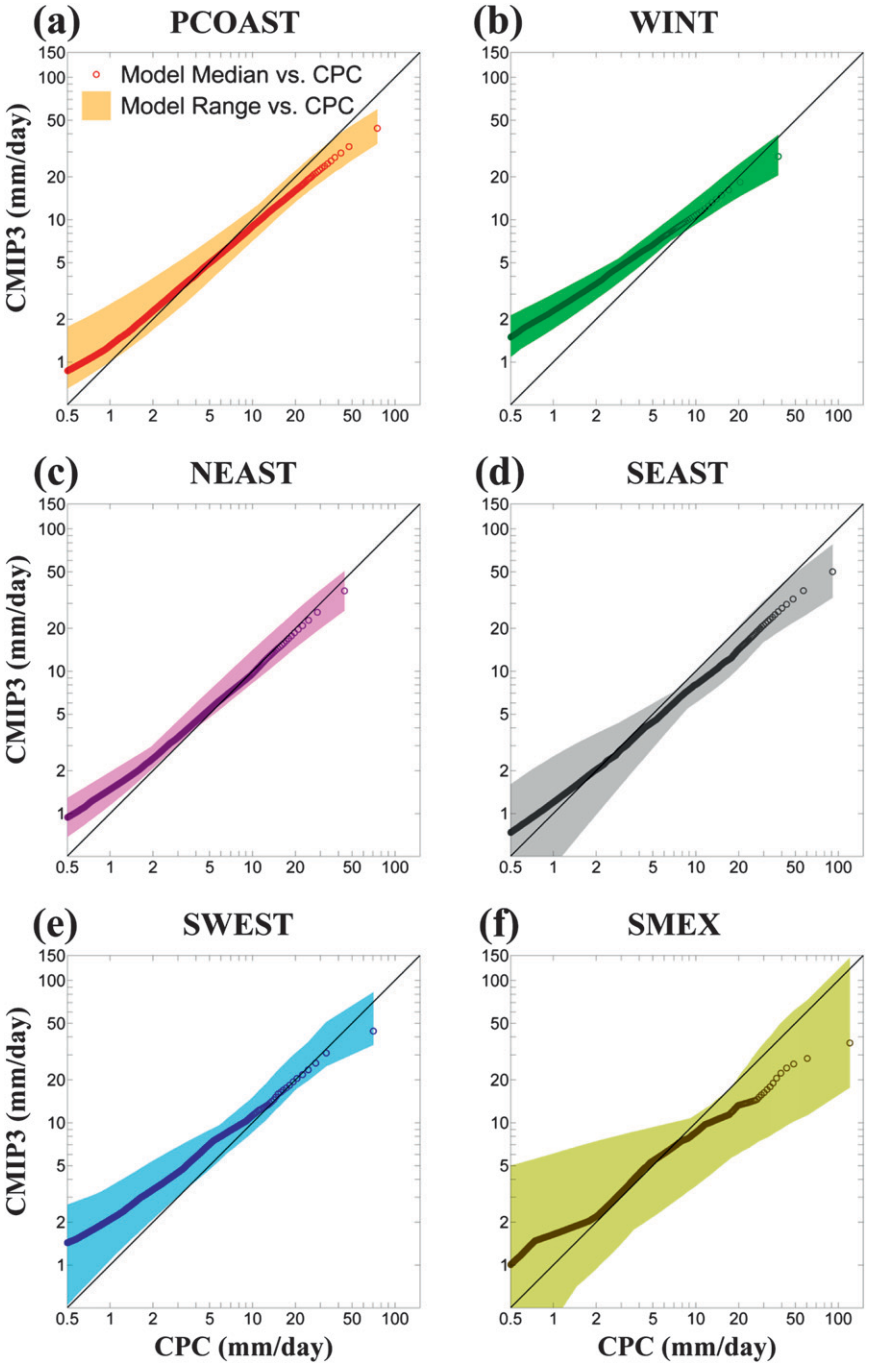

FIG. 5. *Q–Q* plots comparing the annual daily precipitation distribution between the CPC observations and CMIP3 models for each of the regions shown in Fig. 3 (see text for details). In all cases, the circles are showing the model median precipitation value corresponding to each CPC value. The shading is showing the lowest to highest CMIP3 model precipitation value for each corresponding CPC value. Values are plotted only for percentiles for which the CPC precipitation is at least 0.5 mm day^{-1}. The abscissa and ordinate axes are on a logarithmic scale due to the nonlinearity of daily precipitation distributions. The solid black line is a 1:1 line indicating where all data points would fall if there were perfect agreement between the models and observations.

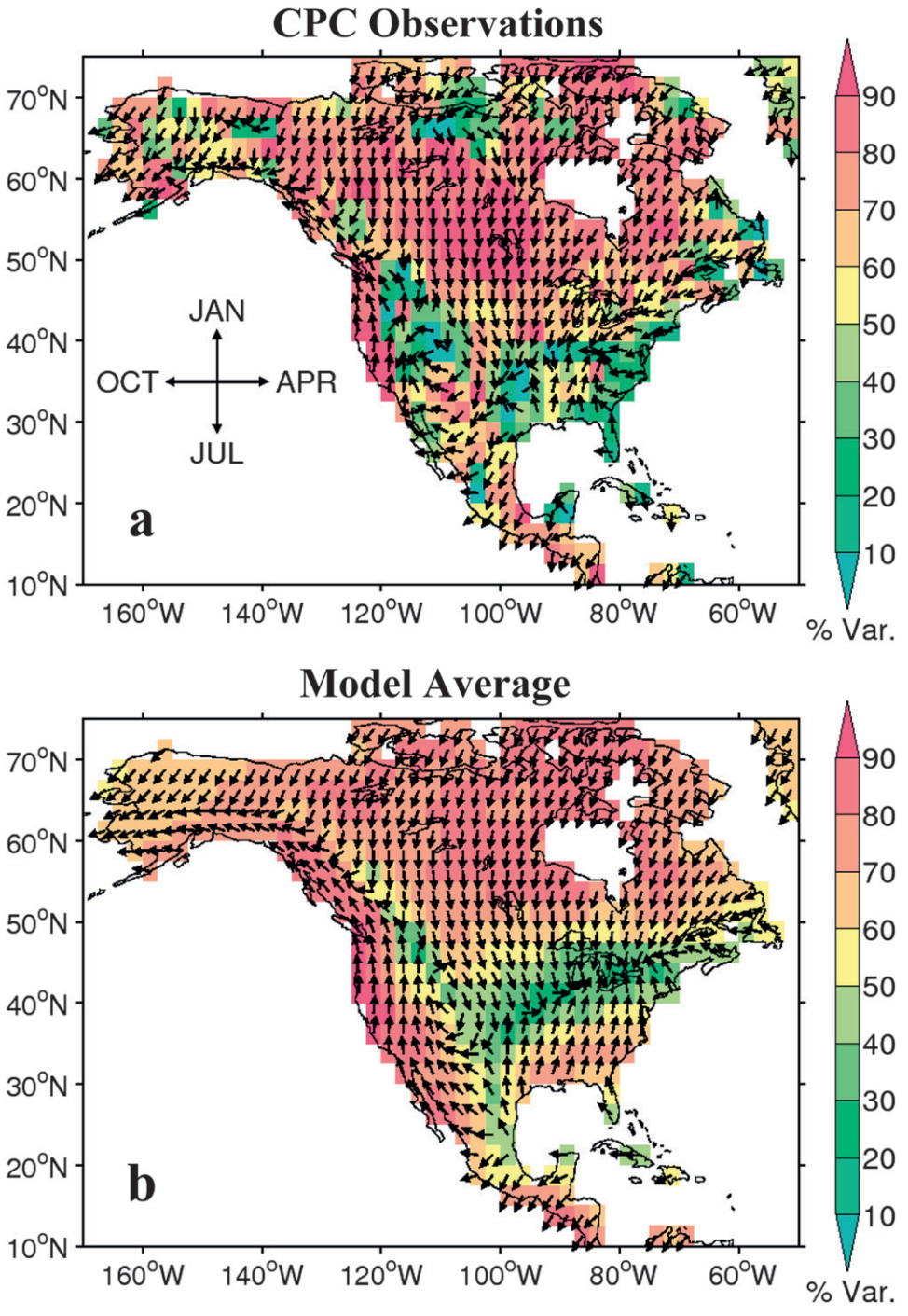

FIG. 6. The seasonal cycle of heavy precipitation, as determined by the first harmonic of the P99M precipitation for each calendar month (see text for details) for (a) the CPC observations and (b) the CMIP3 model average. The vectors point in the direction of the seasonal maximum of P99M objectively determined by the harmonic fit, following the legend shown in (a). Color fills show the percentage of total variance of monthly P99M that the first harmonic explains.

Pacific coast and summer maximum in central North America and southern Mexico, consistent with our results.

4. Physical mechanisms associated with extreme precipitation

The large-scale physical mechanisms associated with extreme precipitation events were analyzed by developing composites of various atmospheric quantities during the most extreme precipitation events at each grid cell. To compute a composite for a grid cell, the dates of the heaviest 21 precipitation events were identified and an atmospheric quantity of interest was averaged over those 21 dates for the entire North American domain, resulting in a map showing the composite spatial structure of that quantity associated with an average extreme event at that grid cell. The number of events was chosen subjectively so that the smallest event would have a probability of occurring approximately once per year, as 21 years of data were used (1979–1999). The 21st wettest event also represents approximately the 99th percentile (the basis of heavy precipitation statistics studied in this paper) when drawn from a sample consisting of just winter [December–February (DJF)] or summer [June–August (JJA)] days. For observations, the CPC product was used to identify the 21 most extreme precipitation events at each grid cell while the NARR was used for the atmospheric quantities that were composited.

In some cases, the atmospheric quantities were first converted to a standardized anomaly at each grid cell before computing the composites, to eliminate the influence that model biases in the mean and variability of the atmospheric quantities would have on the results. The standardized anomaly (or z score) is defined as the anomaly divided by the standard deviation. The climatological mean and standard deviation were computed for a 21-day window centered on the original date (the date corresponding to each of the 21 extreme events) over all years from the period 1980–98. Defining the mean and standard deviation in this way allowed for the z scores to represent anomalies that were with respect to a smoothly varying and seasonally dependent climatology (Hart and Grumm 2001).

As mentioned previously, only 12 CMIP3 models contained all of the variables needed for the composite analysis and therefore only these 12 models were analyzed (see Table 1). An analysis of biases in precipitation statistics using just these 12 models (not shown) led to the same conclusions as those presented in section 3 using all 17 models. Therefore, a direct comparison can be made between the precipitation analysis in section 3 and composite analysis shown here. When comparing composites between NARR and the model average, it should be noted that the model average is actually the composite of 252 extreme events (21 events from 12 different models) while the NARR is the composite of only 21 events. As a consequence of averaging across a larger number of events, the circulation features in the model average will be smoother than in NARR, and this must be taken into consideration when evaluating the realism of the simulated composites. Additionally, the composited quantities are shown over the entire North America domain for all analyzed grid cells in this section. The reader should note that only patterns of composited quantities that are relatively close to the analyzed grid cells (within ~1000 km) are likely to be associated with the extreme events at those grid cells, and that patterns of composited quantities may be influenced by noise or climatology in distant areas.

To characterize the basic large-scale dynamical structure of the atmosphere, composites of pressure at mean sea level (hereafter PMSL) and geopotential height standardized anomalies at 500 mb (hereafter Z500*) were made for various North American grid cells (Figs. 7, 8, 10–12). The geopotential height was not available as a direct quantity from any of the CMIP3 models, so it was calculated by first computing surface pressure (a quantity that was also unavailable from CMIP3 models) using the hydrostatic equation, and then using the hypsometric equation. Although the NARR outputs geopotential height directly, NARR geopotential height was computed in the same way as for the CMIP3 models for the sake of consistency. Differences between geopotential height directly output from NARR and that calculated with the same method as for the CMIP3 models were very small (not shown), suggesting that the method of calculation was satisfactory. The atmospheric levels which were available from the CMIP3 models and used in all computations involving multiple vertical levels in this paper were 1000, 925, 850, 700, 600, 500, 400, 300, and 200 mb, where levels below the surface were omitted.

The composites displayed in this section focus on grid cells where the CMIP3 models either showed substantial biases in P99M precipitation or where P99M precipitation was simulated quite well. A comparison of simulated and observed composites at these grid cells provides insight as to the physical problems with models that might be responsible for biases in heavy precipitation amounts. The first selection of grid cells includes locations where P99M precipitation is severely underestimated by the models in both winter and summer: the Pacific coast near 55°N, the southeast United States, and southern Mexico (Figs. 7 and 8). In comparing the winter composites of PMSL and Z500* between the NARR and model average, the models reasonably

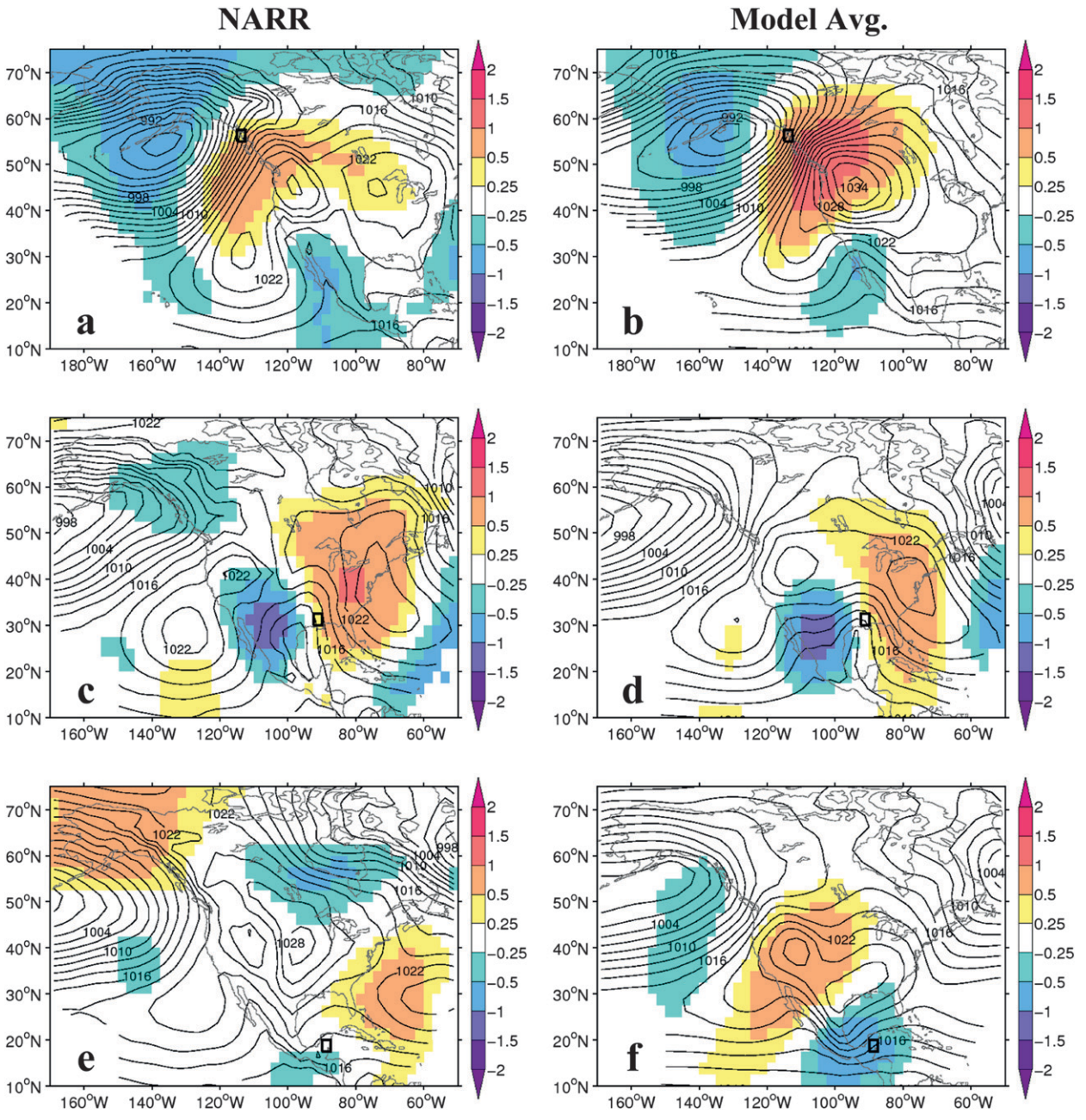

FIG. 7. Composites of pressure at mean sea level (PMSL; hPa, contours) and 500-mb geopotential height standardized anomalies (Z500*; dimensionless, color fills) for the 21 most extreme winter (DJF) precipitation events at selected grid cells (indicated by black rectangles) over which the models severely underestimate P99M precipitation. Sea level pressure is contoured every 2 hPa. (left) Composites based on NARR and (right) those averaged over all CMIP3 models.

simulate the gross atmospheric circulation features associated with extreme events at these grid cells, especially when taking into account the additional smoothing in the model average (Fig. 7). However, the model average composites for the Pacific coast and southern Mexico show stronger circulation features and larger gradients in PMSL and Z500* than is observed (Figs. 7b,f). Composites for a majority of the individual CMIP3 models at these grid cells look very similar to the model average composite, with only few models having stronger or weaker circulation features than the model mean (not shown). Thus, the model average composite for these cases does not appear to be influenced by individual outlier models and is a representative measure

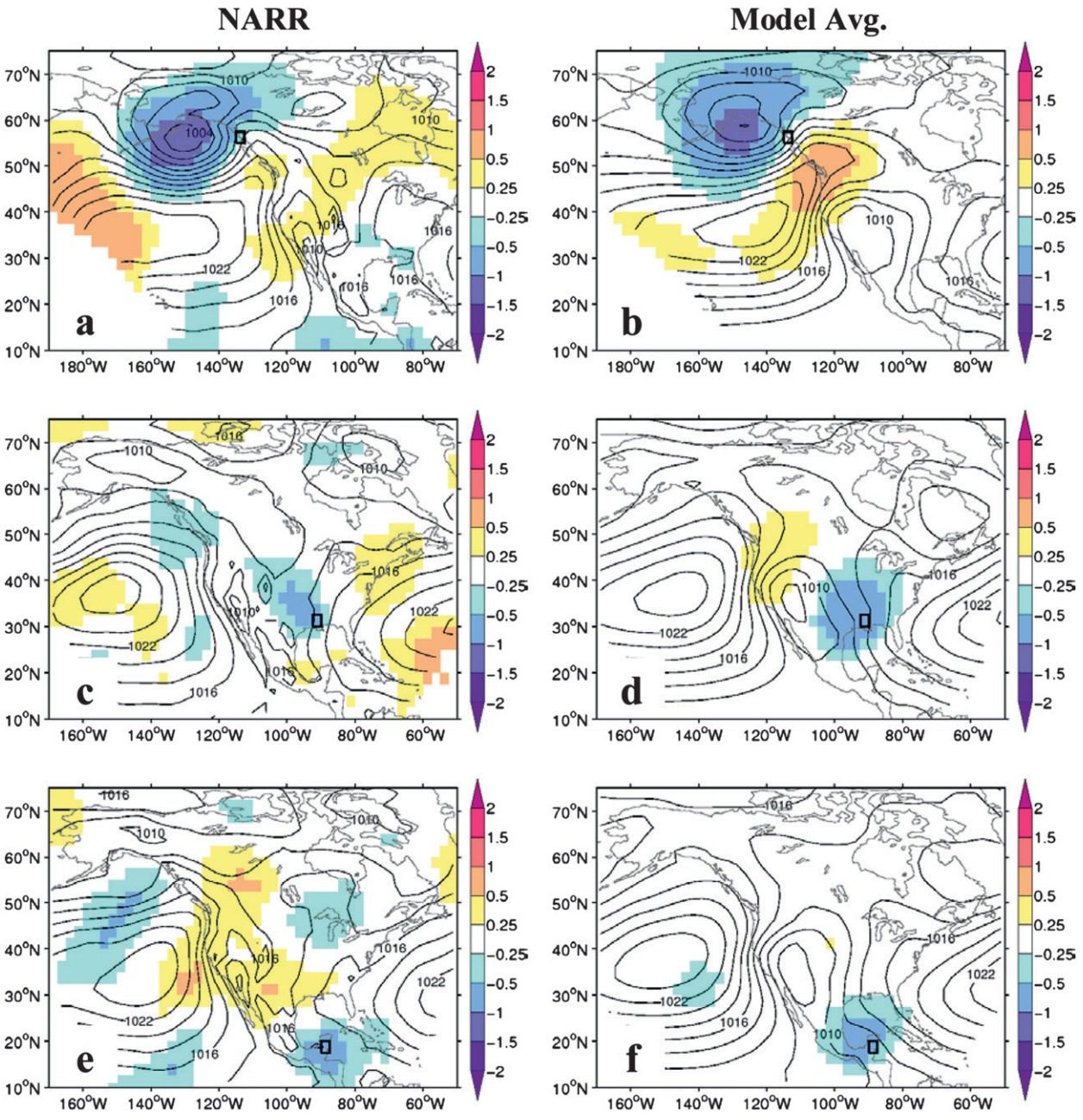

FIG. 8. As in Fig. 7, but for extreme summer (JJA) precipitation events.

of how the bulk of the CMIP3 models perform. This is generally the case for all other grid cells shown in this paper where the model average appears to have biases in circulation features. Composites from different grid cells than the ones shown here within the Pacific coast, southeast United States, and southern Mexico regions have the same characteristics as those shown in Fig. 7 (not shown). In the summer, the observed atmospheric circulation features associated with extreme precipitation at the same grid cells shown in Fig. 7 are much weaker (Figs. 8a,c,e). Furthermore, there is a minimum in Z500* located over or close to the grid cells at low latitudes, suggesting that atmospheric instability and moist convection are important mechanisms for extreme summer precipitation. As in the winter composites, the CMIP3 models reasonably capture the broad atmospheric patterns observed during extreme summer events, with perhaps a slight overestimation of the strength of the circulation features (Figs. 8b,d,f).

Along the Pacific coast, the CMIP3 models underestimate heavy winter precipitation yet the atmospheric

circulation features associated with extreme precipitation events are slightly stronger than observed (Figs. 7a,b), suggesting that other physical deficiencies are present in the models. One likely deficiency is the oversimplified representation of topography by the coarse-resolution models over this mountainous region, which leads to unrealistically light precipitation on the upwind side of mountains. Other studies have shown that climate models of varying spatial resolution and complexity underestimate extreme precipitation in places where it is orographically forced (Iorio et al. 2004; Semmler and Jacob 2004; Wehner et al. 2010), but that higher-resolution simulations are more realistic (Colle and Mass 2000; Iorio et al. 2004; Wehner et al. 2010). Composites of vertically integrated water vapor flux (hereafter VIWVF) and the convergence of VIWVF [hereafter C(VIWVF)], two quantities that are highly relevant to the generation of extreme precipitation (e.g., Trenberth et al. 2003), were also produced for this grid cell (Figs. 9a,b). These composites support that deficiencies in CMIP3 orography are related to heavy precipitation underestimation at this location. In particular, the models underestimate C(VIWVF) over the center of strong convergence associated with extreme events while the magnitudes and orientation of VIWVF vectors are realistic to somewhat weaker than observed (Figs. 9a,b). Additional composite analyses reveal that an underestimation in vertically integrated water vapor itself (hereafter VIWV) and gradients in VIWV near the Pacific coast are the primary cause for underestimations of VIWVF and C(VIWVF) (not shown). Such underestimations of gradients in VIWV are likely a direct result of the oversimplified topography in the CMIP3 models.

In the southeast United States and Mexico, the underestimation of heavy precipitation despite realistic or overly strong circulation features during extreme events is possibly related to problems in simulating convective precipitation. This is supported by the dominance of convective precipitation in these regions, especially during summer (Changnon 2001; Dai 2001; Christian et al. 2003; Riemann-Campe et al. 2009), and the probable link between convective parameterizations and the underestimation of heavy precipitation in climate models (Gutowski et al. 2003; Iorio et al. 2004; May 2004; Emori et al. 2005; Kharin et al. 2007; Wilcox and Donner 2007; Wehner et al. 2010; Li et al. 2012). The northward migration of dry P99M model biases in summer (see Fig. 2) is also consistent with this explanation, as convective precipitation spreads north in summer (Changnon 2001; Dai 2001; Christian et al. 2003; Riemann-Campe et al. 2009), and simulated atmospheric circulation features during extreme summer events in the Midwestern United States are also realistic (not shown). Because tropical cyclones are also an important mechanism for extreme precipitation at low latitudes near the Atlantic Ocean (Rappaport 2000; Lau et al. 2008; Kunkel et al. 2010; Kunkel et al. 2012), the underestimation of heavy precipitation in these regions is possibly also related to the inability of the coarse-resolution CMIP3 models to accurately simulate tropical cyclones (Bengtsson et al. 1995; McClean et al. 2011; Manganello et al. 2012).

In some places, such as the western intermountain regions from Canada through Mexico, the CMIP3 models overestimate the intensity of P99M precipitation during winter (see Figs. 2 and 4). Winter composites of PMSL and Z500* for a selected grid cell in the western United States show that the atmospheric circulation pattern associated with extreme winter events is simulated realistically by the CMIP3 models (Figs. 10a,b). This implies that the overestimation of heavy precipitation at this grid cell is mainly the result of the CMIP3 models oversimplifying the complex topography of western North America. That is, in places where observed precipitation is small because of subsidence on the lee side of mountains, the models simulate too much precipitation because the true terrain pattern is not accurately represented (Colle and Mass 2000). Composites of VIWVF and C(VIWVF) at this location indicate that the models overestimate C(VIWVF) during extreme winter events and that this overestimation is predominantly the result of underestimations in the divergence of low-level (10 m to 500 mb average) winds (not shown). It is possible that such deficiencies in the simulated wind divergence at this location are partly influenced by the unrealistic representation of topography.

In north central Mexico, the observed atmospheric circulation during extreme winter events is characterized by a rather complex pattern in which surface winds originate from the Gulf of Mexico and anomalous midtropospheric winds come from the Pacific Ocean (Fig. 10c). Although the CMIP3 models realistically simulate the main features of this pattern, they slightly overestimate the gradients in PMSL and Z500* (Fig. 10d). Model average composites of VIWVF and C(VIWVF) show substantial biases when compared to NARR for this location (Figs. 9c,d). The overestimations of VIWVF vectors stem from overestimations in low-level wind and VIWV itself, while overestimations in C(VWIVF) result from overestimations in the convergence of low-level wind (not shown). It is possible that the oversimplified representation of the complex topography of Mexico in the models partly influences overestimations in the low-level wind convergence discussed above. However, given that circulation biases are also apparent with composites of PMSL and Z500*, it is likely that some fundamental large-scale deficiency in the atmospheric

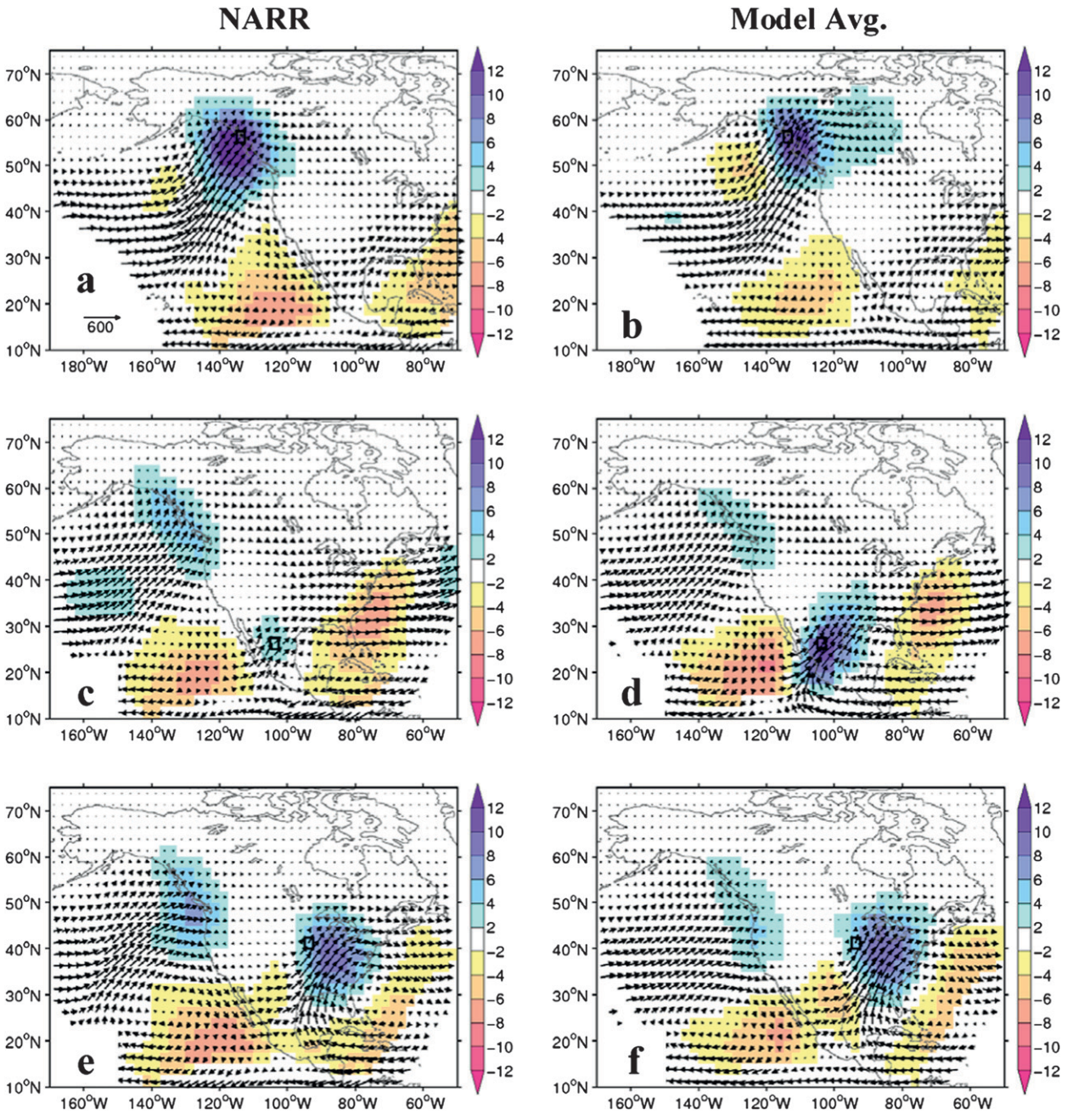

FIG. 9. Composites of vertically integrated water vapor flux (VIWVF; kg m^{-1} s^{-1}, vectors) and the convergence of vertically integrated water vapor flux [C(VIWVF); mm day^{-1}, color fills] for the 21 most extreme winter (DJF) precipitation events at selected grid cells (indicated by black rectangles). The C(VIWVF) was smoothed with a five-point box smoother before plotting. (left) Composites based on NARR and (right) those averaged over all CMIP3 models.

dynamics is present in CMIP3 models during extreme precipitation events over this region.

Composites of PMSL and Z500* are also shown for locations where heavy to extreme precipitation is quantitatively realistic in the CMIP3 models to see if the atmospheric circulation during extreme events is simulated accurately in those places (Figs. 11 and 12). Two such locations are Newfoundland and northern Canada. The atmospheric circulation during extreme events over Newfoundland is qualitatively similar in winter and summer, although gradients of PMSL and Z500* are much weaker in summer (Figs. 11a and 12a). In both seasons, the CMIP3 model average overestimates the strength of the low PMSL associated with the circulation

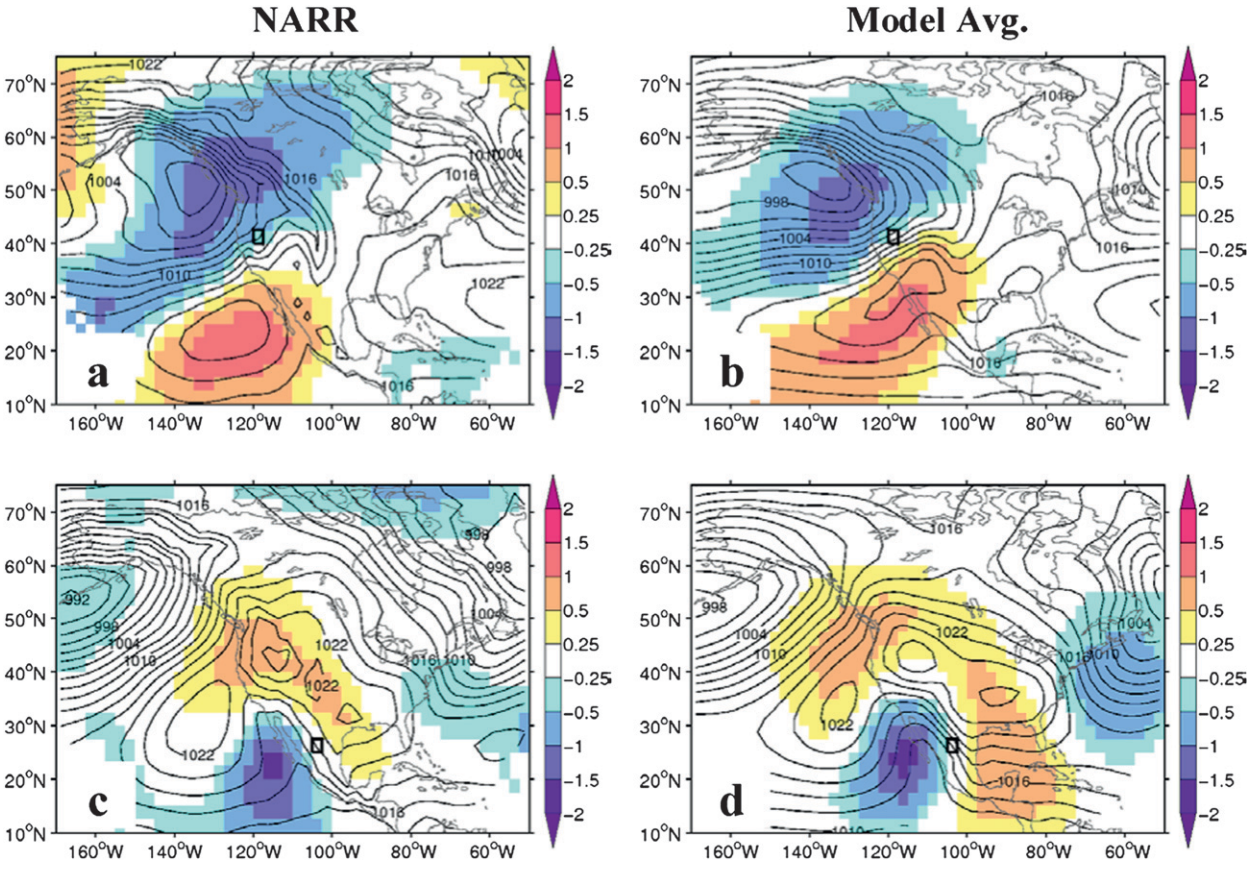

FIG. 10. As in Fig. 7, but for selected grid cells over which models overestimate winter P99M precipitation.

and places the low closer to the grid cell (Figs. 11b and 12b). In winter, the couplet of positive/negative Z500* is also shifted northeast in the models (Fig. 11b). Given that the models generate quite realistic P99M precipitation amounts over this region, it is possible that such errors in the circulation are compensated by other model deficiencies. Such deficiencies may stem from the inability of the models to resolve or accurately simulate some of the processes that generate extreme precipitation in the northeastern part of North America. These processes can include moist convection and tropical cyclones in the warm season (Dai 2001; Christian et al. 2003; Riemann-Campe et al. 2009; Kunkel et al. 2010; Kunkel et al. 2012; Manganello et al. 2012), mesoscale precipitation bands associated with extratropical cyclones (Novak et al. 2004), and other features of the synoptic atmospheric structure that were not explored in this paper (Milrad et al. 2010). The atmospheric circulation patterns during extreme events in northern Canada are interesting in that they appear to result in low-level moisture flow that originates from the Pacific Ocean in winter and Gulf of Mexico in summer (Figs. 11c and 12c). The model average captures this observed seasonal shift in moisture flow rather well, despite having a somewhat different arrangement of low and high PMSL centers in winter and somewhat stronger gradients of PMSL in summer (Figs. 11d and 12d). As was the case with Newfoundland, it is possible that small errors in the simulated circulation over northern Canada are compensated by other physical deficiencies in the models (discussed above), resulting in realistic P99M precipitation.

Composite patterns of low-level wind and standardized anomalies of vertically integrated water vapor (hereafter VIWV*) were computed for extreme winter and summer precipitation events at every grid cell on the North America domain. The values of low-level wind and VIWV* at the center grid cell for each of the composites were then displayed on a map of North America (Fig. 13). This analysis represents a summary of the atmospheric circulation and moisture anomalies associated with extreme events at every grid cell on the domain and is intended to provide a measure of CMIP3 model performance for grid cells that were not explicitly analyzed in Figs. 7–12. It should be noted that because only the local low-level wind associated with extreme events at each grid cell is displayed in Fig. 13, the wind vectors do

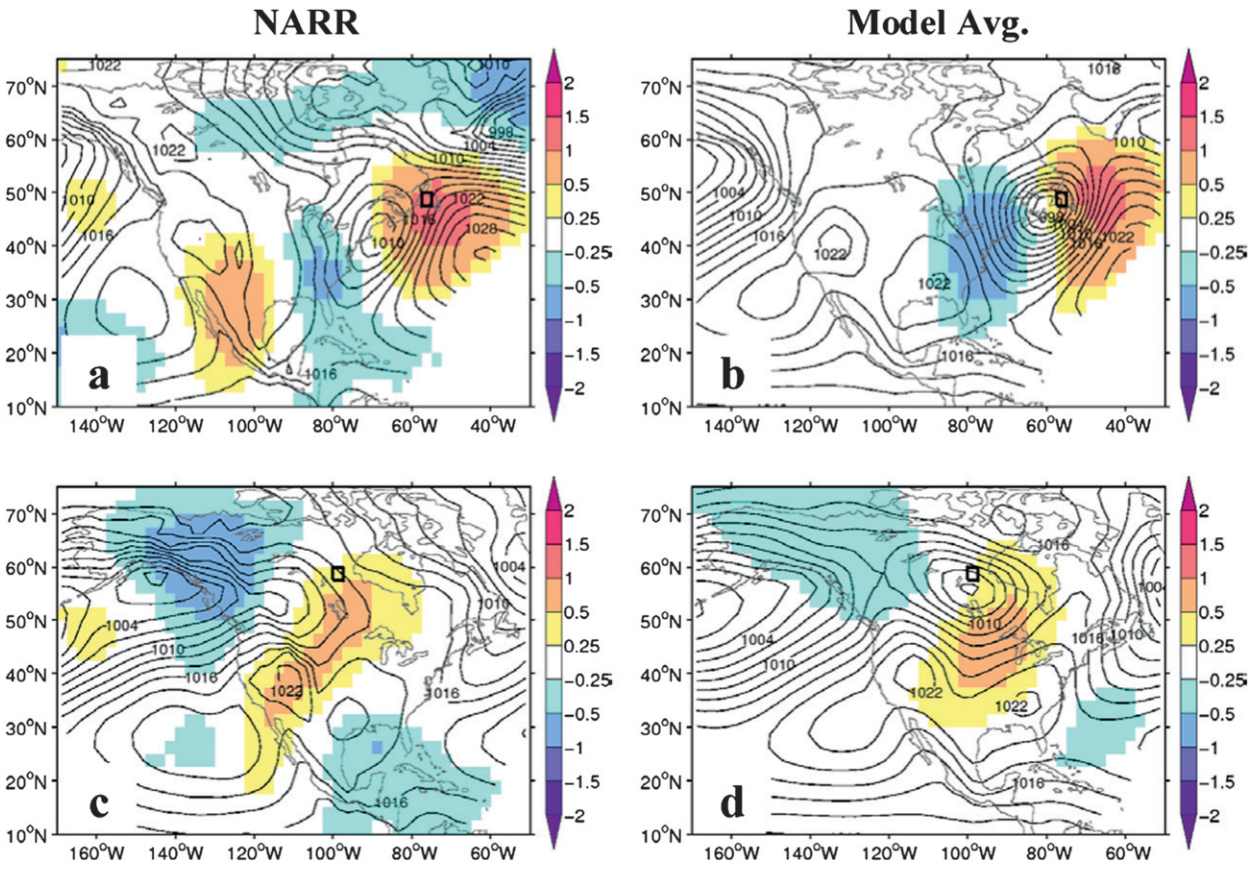

FIG. 11. As in Fig. 7, but for selected grid cells over which models produce realistic winter P99M precipitation.

not always indicate an oceanic moisture source. For instance, the moisture source for extreme winter precipitation events in the Midwestern United States includes both the Gulf of Mexico and western Caribbean, as seen in composites of VIWVF and C(VIWVF) for a Midwest grid cell (Figs. 9e,f), despite local low-level winds being from the southwest (Figs. 13a,b). Nonetheless, the observed patterns of local wind and VIWV* during extreme events are not surprising: winds usually blow the from the south and/or a source of moisture when near the coast, there are positive VIWV* values across the domain, and there are much weaker local winds and VIWV* values during summer as a result of weaker and less organized circulation patterns (Figs. 13a,c). Many of the conclusions that were reached about the ability of CMIP3 models to simulate the observed circulation during extreme events from the analysis of individual grid cells can be seen in Fig. 13. That is, despite being able to reproduce the gross features, the models tend to overestimate the strength of the circulation associated with extreme events over some places. Figure 13 reveals that such overestimations in the circulation are largest along the entire Pacific coast and much of northern and eastern Canada, where VIWV* values are also too high in the models. Over much of northeastern North America, the simulated direction of local wind during extreme events also has small errors (Figs. 13b,d), as was suggested by composites of PMSL and Z500* over Newfoundland (Figs. 11–12). Over many of these regions where the models have biases in simulated circulation, P99M precipitation is realistic or even underestimated, strengthening the point that errors in the simulated circulation during extreme events may be compensated by other physical deficiencies in the models.

In addition to the simple physical quantities shown in Figs. 7–12, other physical quantities were computed that further summarize the complexity of atmospheric circulation and thermodynamic patterns associated with extreme precipitation events. One such quantity is **Q**-vector convergence (hereafter QVC), a metric based on quasigeostrophic theory that quantifies the portion of upward vertical motion explained by synoptic and meso-α-scale forcing (i.e., warm air advection, positive vorticity advection, and large-scale frontogenesis) (Hoskins et al. 1978). Quantitatively, the **Q** vector can be computed with gradients in geopotential height and temperature

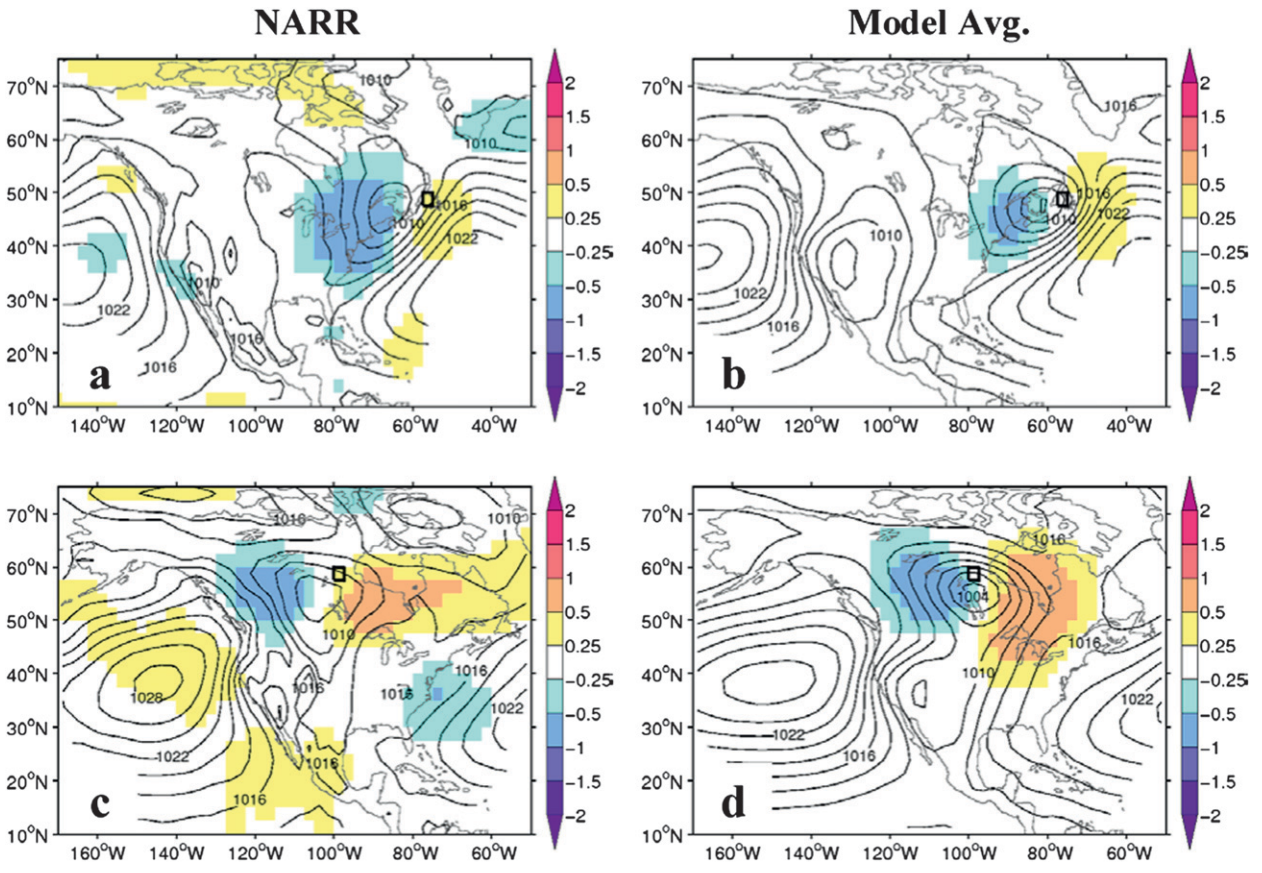

FIG. 12. As in Fig. 11, but for extreme summer (JJA) precipitation events.

at a given atmospheric level (Holton 2004, 168–174). Composites of QVC averaged over the lower troposphere (850, 700, and 600 mb) were analyzed for extreme winter and summer precipitation across the North America domain. The analysis revealed that the CMIP3 models accurately capture the features of QVC associated with extreme events but overestimate the magnitudes of QVC in regions where the large-scale circulation is also overestimated, particularly the northeastern part of the domain (not shown). Such results are consistent with those presented in Figs. 7–13. The lifted index, a quantity that approximately characterizes the atmospheric static stability and thus potential for convective precipitation, was also composited during extreme events. This analysis showed that while the magnitudes of lifted index were sometimes underestimated by the models, patterns of standardized anomalies of lifted index were quite realistic over most of the domain (not shown). This implies that the anomalous thermodynamic structure of the atmosphere during extreme events, partly driven by the large-scale circulation, is simulated well by the CMIP3 models.

5. Summary and conclusions

In this paper, we evaluated various aspects of daily precipitation statistics from an ensemble of 17 CMIP3 models by comparing the model output with gridded observations from the CPC over North America. We found that heavy and extreme precipitation intensities are too light in the models over the southeastern United States, southern Mexico, and along the Pacific coast, and are too heavy in intermountain regions of western North America including north central Mexico. These model biases are quite robust among most or all of the CMIP3 models studied. When looking at the entire daily precipitation distribution, the models overestimate light precipitation intensities and underestimate heavy precipitation intensities to an extent that varies with geographic location. On a positive note, we found that the CMIP3 models generate fairly realistic heavy precipitation in northeastern North America and capture the seasonal cycle of heavy precipitation quite well over parts of the study domain. Our findings are consistent with previous studies that have evaluated global and regional climate models over a wide variety of geographic

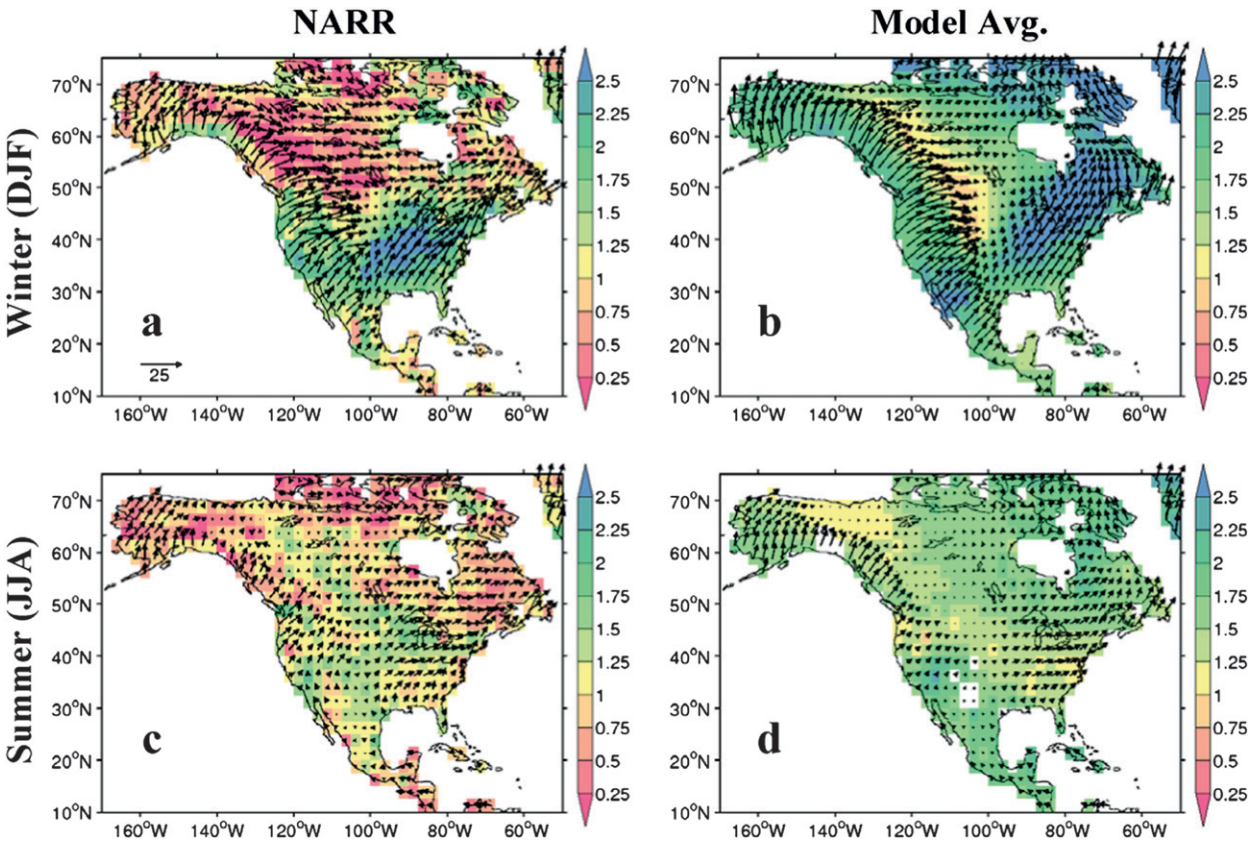

FIG. 13. The average local low-level (10-m to 500-mb average) winds (m s^{-1}, vectors) and vertically integrated water vapor standardized anomalies (VIWV*; dimensionless, color fills) during the 21 most extreme (a),(b) winter and (c),(d) summer precipitation events at every grid cell on the domain, for (left) NARR and (right) the model average. Missing grid cells in (d) are the result of missing specific humidity values for some days in the CSIRO-Mk3.0 model output.

locations, using various observational data sources and different methods to quantify heavy and extreme precipitation.

An analysis of the large-scale physical mechanisms associated with extreme precipitation events was conducted for a subset of the CMIP3 models that were used to study precipitation statistics. We found that the models realistically simulate the gross patterns of sea level pressure and geopotential height anomalies associated with extreme events across most of North America. However, there is a tendency for the models to overestimate gradients in sea level pressure and geopotential height anomalies during extreme events, which in turn results in overestimated low-level winds, column integrated moisture anomalies, and **Q**-vector convergence over parts of the domain. This analysis showed that there is no simple relationship between model biases in circulation strength and biases in heavy precipitation, as the models produced realistic or too strong circulations in regions where heavy precipitation was underestimated, overestimated, or realistic. This suggests that other physical deficiencies in the models are important for model biases in heavy precipitation. Such deficiencies may include problems simulating convective precipitation and tropical cyclones, unrealistically smooth topography as a result of the coarse model resolutions over mountainous regions, and problems simulating mesoscale processes. Previous studies indicate that a combination of increasing the resolution at which climate models are run and adjusting various aspects of convective parameterizations may substantially improve the biases in simulated high-frequency precipitation generated by such physical problems (Colle and Mass 2000; Iorio et al. 2004; Emori et al. 2005; Kimoto et al. 2005; Kharin et al. 2007; Wilcox and Donner 2007; Wehner et al. 2010; Dulière et al. 2011; Li et al. 2012). However, an even better understanding of the physical deficiencies in climate models is necessary to be able to use these models as tools to predict future changes in extreme precipitation events, which have the potential to cause loss of life and property. Such an understanding requires additional studies that evaluate climate model components

in a more detailed and controlled fashion than that presented here.

The results of this paper are encouraging because the CMIP3 models simulate the atmospheric circulations associated with extreme events rather well even though they incorrectly simulate the frequency and intensity of daily precipitation over many places. This suggests that climate models may be useful tools for predicting and understanding future changes in the large scale physical mechanisms associated with extreme precipitation in response to global warming. As the scientific community shifts its attention to CMIP5, it is important that daily precipitation statistics and the large scale physical processes associated with extreme precipitation be evaluated in CMIP5 models as well.

Acknowledgments. This work was funded by a fellowship from the Environmental Protection Agency Science to Achieve Results (EPA STAR) program and a grant (NA09OAR4310109) from the NOAA Climate Program Office. We acknowledge the modeling groups, the Program for Climate Model Diagnosis and Intercomparison (PCMDI), and the WCRP's Working Group on Coupled Modeling (WGCM) for their roles in making available the WCRP CMIP3 multimodel dataset. Support of this dataset is provided by the Office of Science, U.S. Department of Energy. We thank the NOAA Climate Prediction Center for the global gridded precipitation observations and the Climate Diagnostics Center (CDC) for hosting the North American Regional Reanalysis data.

REFERENCES

Alexander, L. V., and J. M. Arblaster, 2009: Assessing trends in observed and modelled climate extremes over Australia in relation to future projections. *Int. J. Climatol.,* **29,** 417–435.

Allan, R. P., and B. J. Soden, 2008: Atmospheric warming and the amplification of precipitation extremes. *Science,* **321,** 1481–1484.

Archambault, H. M., L. F. Bosart, D. Keyser, and A. R. Aiyyer, 2008: Influence of large-scale flow regimes on cool-season precipitation in the northeastern United States. *Mon. Wea. Rev.,* **136,** 2945–2963.

Bengtsson, L., M. Botzet, and M. Esch, 1995: Hurricane-type vortices in a general circulation model. *Tellus,* **47,** 175–196.

Boberg, F., P. Berg, P. Thejll, W. J. Gutowski, and J. H. Christensen, 2009: Improved confidence in climate change projections of precipitation evaluated using daily statistics from the PRUDENCE ensemble. *Climate Dyn.,* **32,** 1097–1106.

Boroneant, C., G. Plaut, F. Giorgi, and X. Bi, 2006: Extreme precipitation over the Maritime Alps and associated weather regimes simulated by a regional climate model: Present-day and future climate scenarios. *Theor. Appl. Climatol.,* **86,** 81–99.

Changnon, S. A., 2001: Thunderstorm rainfall in the conterminous United States. *Bull. Amer. Meteor. Soc.,* **82,** 1925–1940.

Chen, C., and T. Knutson, 2008: On the verification and comparison of extreme rainfall indices from climate models. *J. Climate,* **21,** 1605–1621.

Chen, M., and Coauthors, 2008a: CPC unified gauge-based analysis of global daily precipitation. *Eos, Trans. Amer. Geophys. Union,* **89** (Western Pacific Geophysics Meeting Suppl.), Abstract A24A-05. [Available online at ftp://ftp.cpc.ncep.noaa.gov/precip/CPC_UNI_PRCP/GAUGE_GLB/DOCU/Chen_et_al_2008_Daily_Gauge_Anal.pdf.]

——, and Coauthors, 2008b: Quality control of daily precipitation reports at NOAA/CPC. *Extended Abstracts, 12th Conf. on IOAS-AOLS,* New Orleans, LA, Amer. Meteor. Soc., 3.3. [Available online at http://ams.confex.com/ams/pdfpapers/131381.pdf.]

——, and Coauthors, 2008c: Assessing objective techniques for gauge-based analyses of global daily precipitation. *J. Geophys. Res.,* **113,** D04110, doi:10.1029/2007JD009132.

Christian, H. J., and Coauthors, 2003: Global frequency and distribution of lightning as observed from space by the Optical Transient Detector. *J. Geophys. Res.,* **108,** D14005, doi:10.1029/2002JD002347.

Colle, B. A., and C. F. Mass, 2000: The 5–9 February 1996 flooding event over the Pacific Northwest: Sensitivity studies and evaluation of the MM5 precipitation forecasts. *Mon. Wea. Rev.,* **128,** 593–617.

Dai, A., 2001: Global precipitation and thunderstorm frequencies. Part I: Seasonal and interannual variations. *J. Climate,* **14,** 1092–1111.

Dulière, V., Y. Zhang, and E. P. Salathé Jr., 2011: Extreme precipitation and temperature over the U.S. Pacific Northwest: A comparison between observations, reanalysis data, and regional models. *J. Climate,* **24,** 1950–1964.

Easterling, D. R., G. A. Meehl, C. Parmesan, S. A. Changnon, T. R. Karl, and L. O. Mearns, 2000: Climate extremes: Observations, modeling, and impacts. *Science,* **289,** 2068–2074.

Emori, S., and S. J. Brown, 2005: Dynamic and thermodynamic changes in mean and extreme precipitation under changed climate. *Geophys. Res. Lett.,* **32,** L17706, doi:10.1029/2005GL023272.

——, A. Hasegawa, T. Suzuki, and K. Dairaku, 2005: Validation, parameterization dependence, and future projection of daily precipitation simulated with a high-resolution atmospheric GCM. *Geophys. Res. Lett.,* **32,** L06708, doi:10.1029/2004GL022306.

Frei, C., J. H. Christenson, M. Déqué, D. Jacob, R. G. Jones, and P. L. Vidale, 2003: Daily precipitation statistics in regional climate models: Evaluation and intercomparison for the European Alps. *J. Geophys. Res.,* **108,** D34102, doi:10.1029/2002JD002287.

Gastineau, G., and B. J. Soden, 2011: Evidence for a weakening of tropical surface wind extremes in response to atmospheric warming. *Geophys. Res. Lett.,* **38,** L09706, doi:10.1029/2011GL047138.

Gutowski, W. J., S. G. Decker, R. A. Donavon, Z. Pan, R. W. Arritt, and E. S. Takle, 2003: Temporal–spatial scales of observed and simulated precipitation in central U.S. climate. *J. Climate,* **16,** 3841–3847.

——, and Coauthors, 2008a: Causes of observed changes in extremes and projections of future changes. *Weather and Climate Extremes in a Changing Climate—Regions of Focus: North America, Hawaii, Caribbean, and U.S. Pacific Islands,* T. R. Karl et al., Eds., National Climatic Data Center, 81–116.

——, S. S. Willis, J. C. Patton, B. R. J. Schwedler, R. W. Arritt, and E. S. Takle, 2008b: Changes in extreme, cold-season synoptic precipitation events under global warming. *Geophys. Res. Lett.,* **35,** L20710, doi:10.1029/2008GL035516.

Hart, R. E., and R. H. Grumm, 2001: Using normalized climatological anomalies to rank synoptic-scale events objectively. *Mon. Wea. Rev.,* **129,** 2426–2442.

Higgins, R. W., W. Shi, E. Yarosh, and R. Joyce, 2000: Improved United States precipitation quality control system and analysis. NCEP/Climate Prediction Center Atlas 7, 40 pp. [Available online at http://www.cpc.ncep.noaa.gov/research_papers/ncep_cpc_atlas/7/.]

Holton, J. R., 2004: *An Introduction to Dynamic Meteorology.* 4th ed. Elsevier Academic, 535 pp.

Hoskins, B. J., I. Draghici, and H. C. Davies, 1978: A new look at the ω-equation. *Quart. J. Roy. Meteor. Soc.,* **104,** 31–38.

Iorio, J. P., and Coauthors, 2004: Effects of model resolution and subgrid-scale physics on the simulation of precipitation in the continental United States. *Climate Dyn.,* **23,** 243–258.

Kharin, V. V., and F. W. Zwiers, 2005: Estimating extremes in transient climate change simulations. *J. Climate,* **18,** 1156–1173.

——, ——, X. Zhang, and G. C. Hegerl, 2007: Changes in temperature and precipitation extremes in the IPCC ensemble of global coupled model simulations. *J. Climate,* **20,** 1419–1444.

Kiktev, D., D. M. H. Sexton, L. Alexander, and C. K. Folland, 2003: Comparison of modeled and observed trends in indices of daily climate extremes. *J. Climate,* **16,** 3560–3571.

Kimoto, M., N. Yasutomi, C. Yokoyama, and S. Emori, 2005: Projected changes in precipitation characteristics around Japan under the global warming. *SOLA,* **1,** 85–88.

Kunkel, K. E., D. R. Easterling, D. A. R. Kristovich, B. Gleason, L. Stoecker, and R. Smith, 2010: Recent increases in U.S. heavy precipitation associated with tropical cyclones. *Geophys. Res. Lett.,* **37,** L24706, doi:10.1029/2010GL045164.

——, ——, ——, ——, ——, and ——, 2012: Meteorological causes of the secular variations in observed extreme precipitation events for the conterminous United States. *J. Hydrometeor.,* **13,** 1131–1141.

Lau, K.-M., Y. P. Zhou, and H.-T. Wu, 2008: Have tropical cyclones been feeding more extreme rainfall? *J. Geophys. Res.,* **113,** D23113, doi:10.1029/2008JD009963.

Lenderink, G., and E. van Meijgaard, 2008: Increase in hourly precipitation extremes beyond expectations from temperature changes. *Nat. Geosci.,* **1,** 511–514.

Li, F., W. D. Collins, M. F. Wehner, D. L. Williamson, J. G. Olson, and C. Algieri, 2011: Impact of horizontal resolution on simulation of precipitation extremes in an aqua-planet version of Community Atmospheric Model (CAM3). *Tellus,* **63A,** 884–892.

——, D. Rosa, W. D. Collins, and M. F. Wehner, 2012: ''Super-parameterization'': A better way to simulate regional extreme precipitation? *J. Adv. Model. Earth Syst.,* **4,** M04002, doi:10.1029/2011MS000106.

Lionello, P., and F. Giorgi, 2007: Winter precipitation and cyclones in the Mediterranean region: Future climate scenarios in a regional simulation. *Adv. Geosci.,* **12,** 153–158.

Manganello, J. V., and Coauthors, 2012: Tropical cyclone climatology in a 10-km global atmospheric GCM: Toward weather-resolving climate modeling. *J. Climate,* **25,** 3867–3893.

Marengo, J. A., M. Rusticucci, O. Penalba, and M. Renom, 2010: An intercomparison of observed and simulated extreme rainfall and temperature events during the last half of the twentieth century: Part 2: Historical trends. *Climatic Change,* **98,** 509–529.

May, W., 2004: Simulation of the variability and extremes of daily rainfall during the Indian summer monsoon for present and future times in a global time-slice experiment. *Climate Dyn.,* **22,** 183–204.

McClean, J. L., and Coauthors, 2011: A prototype two-decade fully-coupled fine-resolution CCSM simulation. *Ocean Modell.,* **39,** 10–30.

Meehl, G. A., J. M. Arblaster, and C. Tebaldi, 2005: Understanding future patterns of increased precipitation intensity in climate model simulations. *Geophys. Res. Lett.,* **32,** L18719, doi:10.1029/2005GL023680.

——, C. Covey, T. Delworth, M. Latif, B. McAvaney, J. F. B. Mitchell, R. J. Stouffer, and K. E. Taylor, 2007: The WCRP CMIP3 multi-model dataset: A new era in climate change research. *Bull. Amer. Meteor. Soc.,* **88,** 1383–1394.

Mesinger, F., and Coauthors, 2006: North American Regional Reanalysis. *Bull. Amer. Meteor. Soc.,* **87,** 343–360.

Milrad, S. M., E. H. Atallah, and J. R. Gyakum, 2010: Synoptic typing of extreme cool-season precipitation events at St. John's, Newfoundland, 1979–2005. *Wea. Forecasting,* **25,** 562–586.

Min, S., X. Zhang, F. W. Zwiers, and G. C. Hegerl, 2011: Human contribution to more-intense precipitation extremes. *Nature,* **470,** 378–381.

Novak, D. R., L. F. Bosart, D. Keyser, and J. S. Waldstreicher, 2004: An observational study of cold season–banded precipitation in northeast U.S. cyclones. *Wea. Forecasting,* **19,** 993–1010.

Perkins, S. E., A. J. Pitman, N. J. Holbrook, and J. McAneney, 2007: Evaluation of the AR4 climate models' simulated daily maximum temperature, minimum temperature, and precipitation over Australia using probability density functions. *J. Climate,* **20,** 4356–4376.

Rappaport, E. N., 2000: Loss of life in the United States associated with recent Atlantic tropical cyclones. *Bull. Amer. Meteor. Soc.,* **81,** 2065–2073.

Riemann Campe, K., K. Fraedrich, and F. Lunkeit, 2009: Global climatology of convective available potential energy (CAPE) and convective inhibition (CIN) in ERA-40 reanalysis. *Atmos. Res.,* **93,** 534–545.

Ruiz-Barradas, A., and S. Nigam, 2006: IPCC's twentieth-century climate simulations: Varied representations of North American hydroclimate variability. *J. Climate,* **19,** 4041–4058.

Semmler, T., and D. Jacob, 2004: Modeling extreme precipitation events—A climate change simulation for Europe. *Global Planet. Change,* **44,** 119–127.

Sun, Y., S. Solomon, A. Dai, and R. W. Portmann, 2007: How often will it rain? *J. Climate,* **20,** 4801–4818.

Tomassini, L., and D. Jacob, 2009: Spatial analysis of trends in extreme precipitation events in high-resolution climate model results and observations for Germany. *J. Geophys. Res.,* **114,** D12113, doi:10.1029/2008JD010652.

Trenberth, K. E., A. Dai, R. M. Rasmussen, and D. B. Parsons, 2003: The changing character of precipitation. *Bull. Amer. Meteor. Soc.,* **84,** 1205–1217.

USGS, 2006: Fact sheet: Flood hazards—A national threat. United States Geological Survey, 2 pp. [Available online at http://pubs.usgs.gov/fs/2006/3026/.]

Wehner, M. F., 2013: Very extreme seasonal precipitation in the NARCCAP ensemble: Model performance and projections. *Climate Dyn.,* **40,** 59–80, doi:10.1007/s00382-012-1393-1.

——, R. L. Smith, G. Bala, and P. Duffy, 2010: The effect of horizontal resolution on simulation of very extreme United States

precipitation events in a global atmosphere model. *Climate Dyn.,* **34,** 241–247.

Wilby, R. L., and T. M. L. Wigley, 2002: Future changes in the distribution of daily precipitation totals across North America. *Geophys. Res. Lett.,* **29,** 1135, doi:10.1029/2001GL013048.

Wilcox, E. M., and L. J. Donner, 2007: The frequency of extreme rain events in satellite rain-rate estimates and an atmospheric general circulation model. *J. Climate,* **20,** 53–69.

Wilks, D. S., 2006: *Statistical Methods in the Atmospheric Sciences.* 2nd ed. Elsevier, 627 pp.

Yin, J. H., 2005: A consistent poleward shift of the storm tracks in simulations of 21st century climate. *Geophys. Res. Lett.,* **32,** L18701, doi:10.1029/2005GL023684.

Zwiers, F. W., and V. V. Kharin, 1998: Changes in the extremes of the climate simulated by CCC GCM2 under CO_2 doubling. *J. Climate,* **11,** 2200–2222.